RESEARCH

A comparative investigation on growth, nanostructure and electrical properties of copper oxide thin films as a function of annealing conditions

K. Khojier · H. Savaloni · Z. Sadeghi

Abstract This paper is an attempt to compare the influence of various annealing conditions on growth, nanostructure, surface morphology and electrical properties of copper oxide thin films. Cu thin films of 85 nm thickness were deposited on glass substrate by thermal evaporation method, and then post-annealed at different environments (air and oxygen flow), different temperatures (200–400 °C) and different times (35 and 75 min). X-ray diffraction results showed (Cu_2O) cuprite phase for all annealed samples at 200 and 250 °C and (CuO) tenorite phase for all samples annealed under different conditions at 350 and 400 °C. A complex phase of CuO and Cu_2O was observed for all annealed samples at 300 °C, with exception for the sample annealed with flow of oxygen for 75 min. The atomic force microscopy results showed that surface morphology of the samples was strongly affected by the changes of annealing conditions (i.e., time, temperature and environment). The size of the grains increased with annealing temperature and time, while the samples annealed with oxygen flow showed larger grains than those annealed in air. Two different behaviors with annealing temperature were distinguished for the surface roughness of the samples annealed in the air and those annealed with

flow of oxygen. Resistivity and Hall effect of samples were measured by a four-point probe instrument and a Hall effect investigation system, respectively. The electrical analyses showed that the variations in annealing conditions had a remarkable effect on measured electrical parameters, namely films resistivity, carriers concentration and type, and Hall mobility.

Introduction

Copper oxide can exist in two crystalline phases viz. cuprous oxide or cuprite (Cu_2O) and cupric oxide or tenorite (CuO) [1]. Cu_2O is a p-type semiconductor of cubic structure with a direct band gap of 2.1–2.6 eV, while CuO is a p-type semiconductor having monoclinic structure and an indirect band gap of 1.9–2.1 eV [2]. However, CuO is also reported to possess n-type conductivity [3]. Because of their remarkable properties, both of these materials are widely used in photovoltaic devices [4], solar cells [5], magnetic devices [6] and catalysis [7]. CuO is also used in other various applications, such as gas sensors [5], magnetic storage media [8], solar energy transformation [9], varistors [10].

Many researchers have reported on obtaining copper oxide thin films, using different methods such as sol–gel [11, 12], pulsed magnetron sputtering [13], reactive magnetron sputtering [14], reactive evaporation [15], RF sputtering [16], ion beam sputtering [17], molecular beam epitaxy [18], plasma evaporation [19], and CVD [20], and investigation of various properties of these materials. However, a simple method consisting of deposition of Cu

K. Khojier (✉)
Department of Physics, Chalous Branch, Islamic Azad University, Chalous, Iran
e-mail: khojier@iauc.ac.ir; k_khojier@yahoo.com

H. Savaloni
Department of Physics, University of Tehran, North Kargar Street, Tehran, Iran

Z. Sadeghi
Department of Physics, Faculty of Science, Central Tehran Branch, Islamic Azad University, Tehran, Iran

Springer

thin film and subsequent annealing may be used to produce copper oxide thin films. Figueiredo et al. [3] and Mohemmed Shanid and Abdul Khadar [1] have separately reported on obtaining the copper oxide thin films by this method. They have produced copper oxide thin films by post-annealing of Cu thin films at the air environment and investigated different properties of these layers just as a function of annealing temperature. But, nanostructure and different properties of these films can be affected by other annealing conditions. Therefore, we decided to make use of this method and investigate the influence of different annealing conditions (i.e., annealing temperature, time and environment) on crystallographic structure, surface morphology and electrical properties of the produced samples.

Experimental details

Copper films of 85 nm thickness were deposited on glass substrates (10×10 mm^2 cut from microscope slide) by thermal evaporation from tungsten boat. The purity of the copper was 99.998 %. An Edwards (Edwards E19 A3) coating plant was used. Film thickness and deposition rate were measured using a quartz crystal deposition rate controller (Sigma Instruments, SQM- 160, USA) positioned close to the substrate. Deposition angle and deposition rate were $15°$ and 3 Å/s, while base pressure was 2×10^{-5} -mbar. Post-annealing of the Cu/glass films was performed by a horizontal tube furnace at five different temperatures of 200, 250, 300, 350 and 400 °C in the air environment and oxygen flow of 200 sccm. Two annealing times of 35 and 75 min were used. The samples reached their target temperature with a thermal gradient of 7 °/min. Prior to deposition, all substrates were ultrasonically cleaned in heated acetone and then ethanol. Crystallographic information of the produced samples was obtained using a Philips XRD X'pert MPD Diffractometer (Cu Kα radiation) with a step size of 0.02° and count time of 1 s per step. Surface morphology and roughness of the samples were obtained by means of AFM (Park Scientific) analysis with a scan rate of 1 Hz and a scan size of 1×1 μm^2. A four-point probe instrument and a Hall effect system with a magnetic field strength of 0.2 T were employed for resistivity measurements and Hall effect analysis, respectively.

Results and discussion

Crystallographic structure

XRD results for all samples are given in Table 1, and the XRD patterns of selected samples (annealed in the air and oxygen flow for 75 min) are shown in Fig. 1. X-ray diffraction pattern of an annealed samples at 200 °C in the air environment for 35 min (sample no. C1) showed one peak that can be related to Cu$_2$O(111) crystallographic orientation (with reference to JCPDS card no.: 05-667, $2\theta = 36.419°$, system: cubic and space group: 224). By increasing the annealing temperature to 250 °C (sample no. C2), the intensity of Cu$_2$O(111) peak was increased.

With annealing at 300 °C (sample no. 3), the intensity of this peak (Cu$_2$O(111)) is decreased, while two other peaks that can be attributed to crystallographic orientations CuO(-111) and CuO(111) are appeared (with respect to JCPDS cards no.: 45-0937, $2\theta = 35.496°$ and no.: 48-548, $2\theta = 38.709°$, system monoclinic and space group: 15). In the XRD pattern of annealed sample at 350 °C (sample no. C4), the Cu$_2$O(111) disappeared and the intensity of CuO(-111) and CuO(111) peaks increased. At 400 °C annealing temperature, the intensities of these two peaks are increased. From these results, it can be deduced that Cu$_2$O or cuprous oxide phase is formed at lower annealing temperatures of 200 and 250 °C, while at higher annealing temperatures of 350 and 400 °C CuO or cupric oxide phase is formed. A mixture of these two phases (i.e., Cu$_2$O and CuO) is presented at annealing temperature of 300 °C. Figueiredo et al. [3] have also reported similar results for their films deposited by electron beam and post-annealed in air for 30 min.

The above-mentioned behavior was observed for almost all samples produced under different conditions, however, with some diversions as follows:

a   The intensities of diffraction peaks were higher for those samples annealed at 200, 250, 350 and 400 °C with flow of oxygen relative to those annealed in air.
b   When annealing time increased to 75 min, the diffraction peaks of samples annealed at 200, 250, 350 and 400 °C showed an increase in the intensity and reduction of the FWHM, indicative of the growth of larger grains (coherently diffracting domains).
c   The sample annealed at 300 °C with flow of oxygen for 75 min (sample no. C18) showed only CuO phase, while the same sample annealed for shorter time of 35 min showed both CuO and Cu$_2$O phases.

Therefore, it may be concluded that the phase transition of copper oxide films produced in this work is directly related to the annealing temperature, environment and time. On the other hand, a higher presence of oxygen and more annealing time promote an oxidation at lower temperatures. For this reason, there was no Cu$_2$O phase in the sample which was sintered at 300 °C in O$_2$ environment for 75 min.

Crystallite size (coherently diffracting domains) D was obtained by applying the Scherrer formula ($D = k\lambda/B\cos\theta$), where k is unity, $\lambda = 1.54248$ Å, θ is the peak

Table 1 Detail of nano-structural results of Cu/glass thin films annealed at different conditions (obtained from XRD and AFM analyses)

Information of samples				XRD analysis			AFM analysis		
No.	T (°C) ±5	Env.	t (min) ±1	Phase	(hkl) 2θ (°)	Intensity (cps) D (nm)[a]	D (nm) ±2	Roughness (Å) ±1	
								rms	R$_{ave.}$
C1	200	Air	35	Cu$_2$O	(111) 36.43	14 14	19	84	67
C2	250	Air	35	Cu$_2$O	(111) 36.43	18 22	29	72	61
C3	300	Air	35	CuO/Cu$_2$O/CuO	(−111)/(111)/(111) 35.51/36.45/38.71	15/13/17 47	61	69	60
C4	350	Air	35	CuO	(−111)/(111) 35.53/38.73	17/21 49	72	75	66
C5	400	Air	35	CuO	(−111)/(111) 35.51/38.73	19/23 56	75	81	65
C6	200	O$_2$	35	Cu$_2$O	(111) 36.45	18 16	22	73	55
C7	250	O$_2$	35	Cu$_2$O	(111) 36.43	20 28	39	82	63
C8	300	O$_2$	35	CuO/Cu$_2$O/CuO	(−111)/(111)/(111) 35.51/36.46/38.73	19/13/21 54	70	95	77
C9	350	O$_2$	35	CuO	(−111)/(111) 35.51/38.71	21/24 57	78	69	55
C10	400	O$_2$	35	CuO	(−111)/(111) 35.53/38.73	23/27 65	79	66	51
C11	200	Air	75	Cu$_2$O	(111) 36.47	21 20	26	114	89
C12	250	Air	75	Cu$_2$O	(111) 36.47	26 39	43	103	81
C13	300	Air	75	CuO/Cu$_2$O/CuO	(−111)/(111)/(111) 35.53/36.45/38.73	24/14/27 69	92	96	76
C14	350	Air	75	CuO	(−111)/(111) 35.55/38.75	25/28 76	99	104	80
C15	400	Air	75	CuO	(−111)/(111) 35.55/38.75	24/31 82	105	109	84
C16	200	O$_2$	75	Cu$_2$O	(111) 36.47	23 23	35	98	75
C17	250	O$_2$	75	Cu$_2$O	(111) 36.49	28 41	51	112	91
C18	300	O$_2$	75	CuO	(−111)/(111) 35.55/38.75	26/30 76	100	139	107
C19	350	O$_2$	75	CuO	(−111)/(111) 35.55/38.77	25/31 81	104	102	97
C20	400	O$_2$	75	CuO	(−111)/(111) 35.57/38.75	23/37 91	111	93	73

T is the annealing temperature

[a] Obtained by Scherrer formula for main peaks with higher intensity

Fig. 1 XRD patterns of annealed Cu/glass thin films in: **a** air and **b** oxygen for 75 min
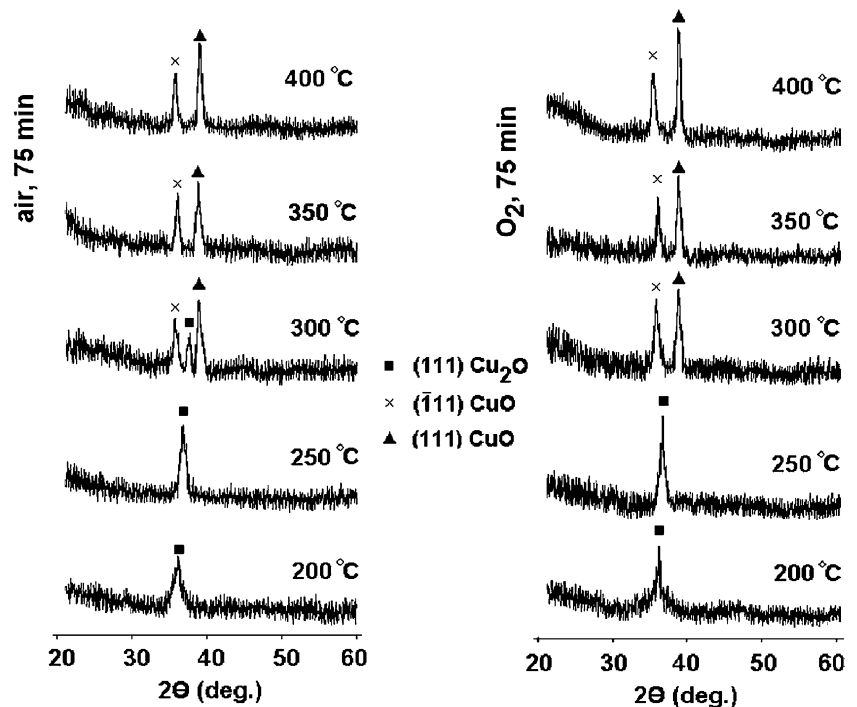
position in radian, and B is calculated from the full width at half maximum of the dominant peak, as $B^2 = B_M^2 - B_s^2$ (B_M is FWHM of the sample and B_S is FWHM of the standard sample) [21]. The crystallite size (coherently diffracting domains) results are given in column 7 of Table 1. The results show that grain size increases with annealing temperature, and the films annealed with oxygen flow for longer time have larger grains. The increase in grain size with annealing temperature is clearly due to higher activation energy which causes higher diffusion rate; however, the larger grains obtained for annealing with flow of oxygen relative to those annealed in air can be due to the fact that air apart from oxygen consists of nitrogen and other gases or contaminants that are usually embedded between grains and stop grains from growing larger [22, 23].

Surface morphology

2D AFM images of selected samples (i.e., samples annealed at 200, 300, 400 °C in the air and oxygen flow for 75 min) are shown in Fig. 2a–f. Grain sizes of all samples were measured from 2D AFM images using JMicrovision Code. Results are given in column 8 of Table 1. These results show that the grain size increases with annealing temperature and when samples annealed with flow of oxygen are compared with those annealed in air, it can be observed that the formers contain larger grains.

Figure 3 depicts the 3D AFM images of selected samples, while rms and average roughness of films obtained

from AFM analysis are given in columns 9 and 10 of Table 1. These results show that for both annealing environments, namely air and oxygen film, surface roughness increases with annealing time for all annealing temperatures used in this work. This can be due to the fact that at longer annealing time, atoms can move more and fill/ remove the defects of different types (i.e., voids, interstitials and other types), hence larger grains may form as mentioned in column 8 of Table 1. In addition, by formation of larger grains usually the valleys between the grains become wider and deeper (i.e., grooving effect [24, 25]), hence surface roughness increases. Moreover, two different behaviors can be distinguished for the samples annealed in the air and those annealed with flow of oxygen. The samples annealed in the air show a minimum surface roughness at 300 °C annealing temperature, while those annealed with flow of oxygen show a maximum value at this temperature.

Concentration of carriers and Hall mobility

The Hall's effect is important, because it enables us to make measures of mobility and concentration of carriers, and gives insight into the mechanism of conductivity in semiconductors. Figs. 4 and 5 illustrate the variation of carrier concentration and Hall mobility of our samples, respectively. The numerical data and the type of carriers are also given in Table 2. Results (Table 2, column 6) show p-type conductivity for samples with Cu_2O structure, while samples with CuO structure have n-type

Fig. 2 2D AFM images of selected Cu/glass samples annealed at different temperatures and in different environments for 75 min: a 200 °C, air; b 300 °C, air; c 400 °C, air; d 200 °C, oxygen flow; e 300 °C, oxygen flow; f 400 °C, oxygen flow
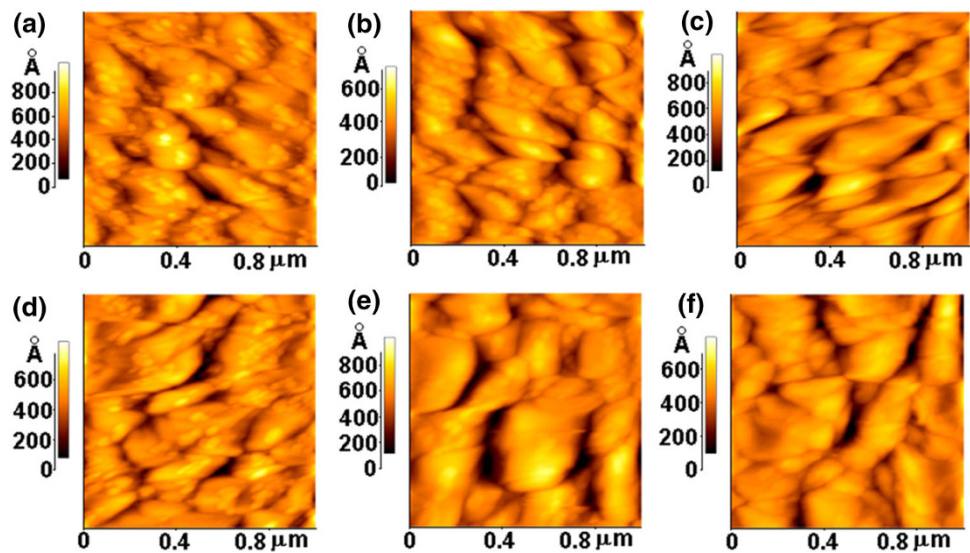
Fig. 3 3D AFM images of selected Cu/glass samples annealed at different temperatures and in different environments for 75 min: a 200 °C, air; b 300 °C, air; c 400 °C, air; d 200 °C, oxygen flow; e 300 °C, oxygen flow; f 400 °C, oxygen flow
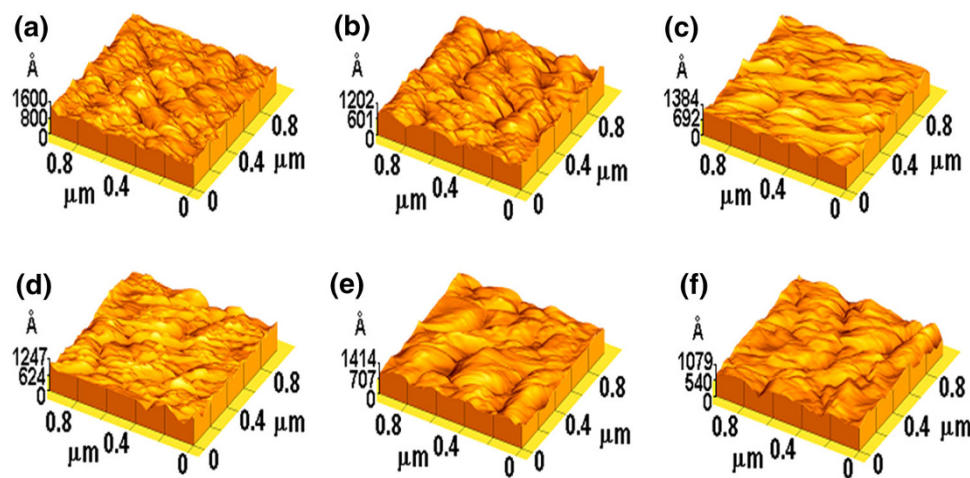

conductivity. Figure 5 and Table 2 (column 7) show that the carrier concentration decreases with increasing the annealing temperature from 200 to 250 °C, while it increases with annealing temperature at higher temperatures. This is true for all samples regardless of their annealing environment or the annealing time. The comparison of these results with the phase identification of the samples given in column 5 of Table 1 suggests that this observation may be related to the crystallographic structure changes of the samples with annealing temperature which in turn is related to the carrier type in the samples (i.e., change from Cu_2O (p-type carrier) to CuO (n-type carrier)).

The variation of Hall mobility for all samples produced in this work is given in column 8 of Table 2 and Fig. 5. From these results and the results given in Table 1, for crystallographic structure of the samples, it can be deduced that these variations are related to the carrier concentration as discussed above, hence are directly influenced by the film crystallographic structure (phase). Consequently, there exists a correlation between the results obtained for carrier concentration, Hall mobility and the crystallographic structure (phase) of the samples produced in this work.

Resistivity

Results of DC resistivity measurement obtained using a four-point probe instrument is discussed in this section. To investigate the influence of possible (low frequency) charging effects at the electrical contacts and leads, current–voltage (I–V) curves were recorded in both increasing and decreasing increments of voltage. The results of the measurements in the decreasing direction of the voltage are not shown as they matched the results in the increasing voltage direction and only clutter the figure unnecessarily. Linear I–V curves were obtained for all samples; independent of the scan direction, there was no indication of
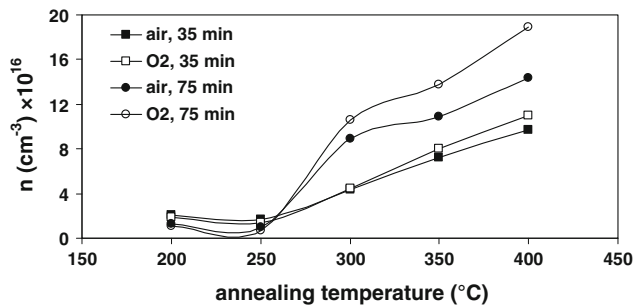
Fig. 4 Variation in carrier concentration of the samples produced at different annealing times and in different environments as a function of annealing temperature (the lines are guides to the eyes)
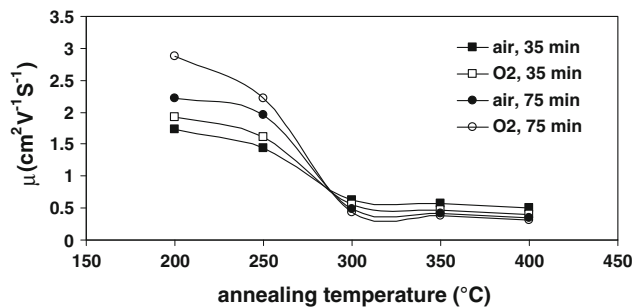
Fig. 5 Variation in Hall mobility of the samples produced at different annealing times and in different environments as a function of annealing temperature (the lines are guides to the eyes)

hysteresis effect. To investigate the anisotropy effect in these samples, the I–V curve measurements were also carried out in four different directions on the samples, namely two vertical (along the sample length and normal to the length) and two diagonal directions. Figure 6 depicts the results of I–V curves for selected samples that were heated in air for 35 min as a function of annealing temperature, while the values of average resistivity for all samples measured at room temperature are given in column 5 of Table 2 and Fig. 7. The results show that resistivity increases with annealing temperature up to 300 °C and decreases at higher annealing temperatures. The variation of the resistivity of our samples again regardless of their annealing environment and annealing time shows a peak value for the samples annealed at 300 °C. Consulting the crystallographic structure (Table 1, column 5) and carrier type (Table 2, column 6) indicates that at this temperature the samples contain a mixture of two phases with two different types of carriers, namely Cu_2O (p-type) and CuO (n-type), though the final identification in Table 2 for the carrier type of these samples is given as p-type. The increased resistivity of these samples could be due to existence of these two different types of carriers in these samples that act in two different directions.

A similar variation of resistivity for films produced by e-beam deposition and subsequent annealing in air for 30 min is reported by Figueiredo et al. [3].

Table 2 Electrical properties results of Cu/glass thin films annealed at different conditions (measured by four-point probe instrument and Hall effect investigation system)

No.	T (°C) ±5	Env.	t (min) ±1	ρ (Ω cm)	Carriers type	n (cm^{-3}) ×10^{16}	μ (cm^2 V^{-1} S^{-1})
C1	200	Air	35	104.0 ± 4	p	2.1 ± 0.08	1.73 ± 0.06
C2	250	Air	35	225.3 ± 9	p	1.7 ± 0.06	1.43 ± 0.05
C3	300	Air	35	425.6 ± 17	p	4.4 ± 0.16	0.62 ± 0.02
C4	350	Air	35	311.3 ± 12	n	7.2 ± 0.28	0.57 ± 0.02
C5	400	Air	35	138.7 ± 5	n	9.7 ± 0.36	0.51 ± 0.02
C6	200	O$_2$	35	122.4 ± 4	p	1.9 ± 0.07	1.93 ± 0.07
C7	250	O$_2$	35	241.8 ± 10	p	1.4 ± 0.05	1.61 ± 0.06
C8	300	O$_2$	35	485.4 ± 17	p	4.5 ± 0.17	0.56 ± 0.02
C9	350	O$_2$	35	301.9 ± 12	n	7.4 ± 0.30	0.47 ± 0.02
C10	400	O$_2$	35	126.9 ± 5	n	10.1 ± 0.44	0.40 ± 0.02
C11	200	Air	75	145.3 ± 5	p	1.3 ± 0.05	2.21 ± 0.08
C12	250	Air	75	275.2 ± 9	p	1.0 ± 0.04	1.96 ± 0.07
C13	300	Air	75	519.1 ± 20	p	8.9 ± 0.32	0.49 ± 0.02
C14	350	Air	75	294.4 ± 12	n	10.9 ± 0.50	0.42 ± 0.02
C15	400	Air	75	112.8 ± 4	n	14.4 ± 0.56	0.35 ± 0.01
C16	200	O$_2$	75	183.6 ± 5	p	1.1 ± 0.04	2.87 ± 0.11
C17	250	O$_2$	75	310.9 ± 12	p	0.7 ± 0.28	2.22 ± 0.08
C18	300	O$_2$	75	504.1 ± 20	n	10.6 ± 0.40	0.43 ± 0.02
C19	350	O$_2$	75	291.6 ± 11	n	12.4 ± 0.50	0.38 ± 0.01
C20	400	O$_2$	75	103.1 ± 4	n	18.9 ± 0.72	0.31 ± 0.01

T is the annealing temperature
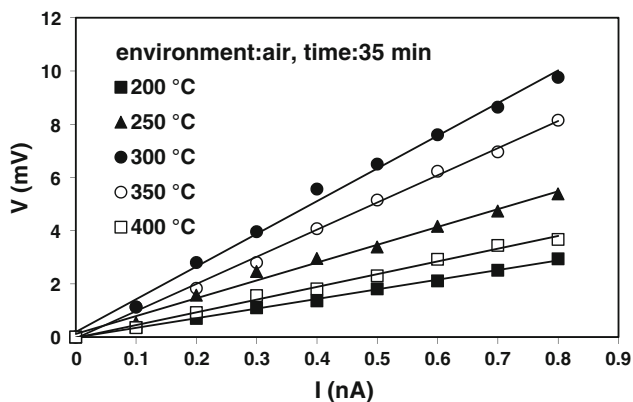
Fig. 6 *I–V* curves for Cu/glass thin films annealed in air for 35 min
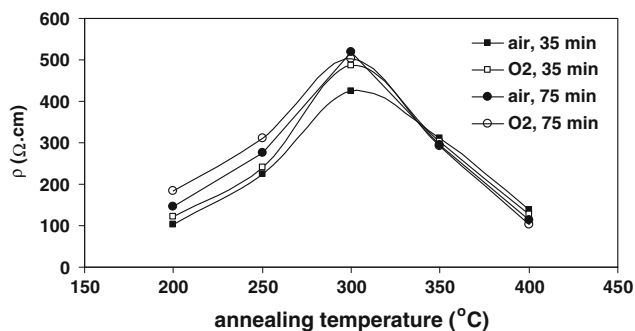
Fig. 7 Variation in resistivity of Cu/glass thin films annealed at different times and in different environments as a function of annealing temperature (the lines are guides to the eyes)

Conclusion

Cu thin films of 85 nm thickness were produced by thermal evaporation on glass substrates. The samples were post-annealed at different temperatures (200-400 °C), different environments (air and flow of oxygen) and different annealing times (35 and 75 min). Crystallographic and morphological investigations were carried out using XRD and AFM analyses, respectively. Resistivity and Hall mobility and carrier concentration of samples were obtained by means of four-point probe and Hall effect investigation instrument separately. Two different phases of copper oxide films, namely Cu_2O and CuO, were observed at lower temperatures (up to 250 °C) and higher temperatures (350 and 400 °C) for all samples, respectively, while at the transition annealing temperature of 300 °C a mixture of both of these phases was obtained for all samples except that annealed with flow of oxygen and for 75 min. Grain sizes obtained from AFM images indicated that the grain size increased with annealing temperature and annealing time, while those annealed with flow of oxygen produced larger grains than those processed in air. Samples annealed in the air showed a minimum surface roughness at 300 °C annealing temperature, while those annealed with flow of oxygen showed a maximum surface roughness at this annealing temperature. This phenomenon may be related to the crystallographic structure of these films, so that those annealed at this certain temperature and in air contain both CuO and Cu_2O grains, whereas those annealed in the oxygen flow (at 300 °C) contain only CuO grains (particularly at increased annealing time of 75 min) or much less amount of Cu_2O (35 min annealing time). This can also be deduced from the ratio of intensities of the peaks of Cu_2O to CuO for these samples (Table 1, column 7), hence distribution of smaller grains (lower intensities of three peaks in the XRD pattern) causes almost a uniform surface (minimum surface roughness) while large grains (higher intensities of two peaks in the XRD pattern) produce a rough surface. In fact, our discussion emphasis is on the distribution of smaller Cu_2O grains among the CuO grains. The electrical results showed n-type conductivity for CuO phase and p-type conductivity for Cu_2O phase. The variations in the resistivity, concentration of carriers and Hall mobility showed a direct correlation with the crystallographic phase changes of the samples as a function of annealing temperature regardless of annealing time and annealing environment.

Conflict of interest The authors declare that they have no competing interests.

Author contribution All authors provided the same contributions in this article. All authors read and approved the final manuscript.

References

1. Mohemmed Shanid, N.A., Abdul Khadar, M.: Evolution of nanostructure, phase transition and band gap tailoring in oxidized Cu thin films. Thin Solid Films **516**, 6245–6252 (2008)
2. Ray, S.C.: Preparation of copper oxide thin film by the sol–gel-like dip technique and study of their structural and optical properties. Sol. Energy Mater. Sol. Cells **68**, 307–312 (2001)
3. Figueiredo, V., Elangovan, E., Goncalves, G., Barquinha, P., Pereira, L., Franco, N., Alves, E., Martins, R., Fortunato, E.: Effect of post-annealing on the properties of copper oxide thin films obtained from the oxidation of evaporated metallic copper. Appl. Surf. Sci. **254**, 3949–3954 (2008)
4. Koffyberg, F.P., Benko, F.A.: A photoelectrochemical determination of the position of the conduction and valence band edges of p-type CuO. J. Appl. Phys. **53**, 1173–1175 (1982)
5. Serin, N., Serin, T., Horzum, S., Celik, Y.: Annealing effects on the properties of copper oxide thin films prepared by chemical deposition. Semicond. Sci. Technol. **20**, 398–401 (2005)

6. Gan, Z.H., Yu, G.Q., Tay, B.K., Tan, C.M., Zhao, Z.W., Fu, Y.Q.: Preparation and characterization of copper oxide thin films deposited by filtered cathodic vacuum arc. J. Phys. D Appl. Phys. **37**, 81–85 (2005)

7. Kari Brown, E.R., Choi, K.: Synthesis and characterization of transparent nanocrystalline Cu_2O films and their conversion to CuO films. Chem. Commun. **31**, 3311–3313 (2006)

8. Borzi, R.A., Stewart, S.J., Mercader, R.C., Punte, G., Garcia, F.: Magnetic behavior of nanosized cupric oxide. J. Magn. Magn. Mater. **226–230**, 1513–1515 (2001)

9. Balamurugan, B., Mehta, B.R., Avasthi, D.K., Singh, F., Arora, A.K., Rajalakshmi, M., Raghavan, G., Tyagi, A.K., Sivaprasad, S.M.: Modifying the nanocrystalline characteristics-structure, size, and surface states of copper oxide thin films by high-energy heavy-ion irradiation. J. Appl. Phys. **92**, 3304–3310 (2002)

10. Wang, W., Liu, Z., Liu, Y., Xu, C., Zheng, C., Wang, G.: A simple wet-chemical synthesis and characterization of CuO nanorods. Appl. Phys. A **76**, 417–420 (2003)

11. Nair, M.T.S., Guerrero, L., Arenas, O.L., Nair, P.K.: Chemically deposited copper oxide thin films: structural, optical and electrical characteristics. Appl. Surf. Sci. **150**, 143–151 (1999)

12. Oral, A.Y., Mensur, E., Aslan, M.H., Basaran, E.: The preparation of copper(II) oxide thin films and the study of their microstructures and optical properties. Mater. Chem. Phys. **83**, 140–144 (2004)

13. Alkoy, E.M., Kelly, P.J.: The structure and properties of copper oxide and copper aluminium oxide coatings prepared by pulsed magnetron sputtering of powder targets. Vacuum **79**, 221–230 (2005)

14. Pierson, J.F., Thobor-Keck, A., Billard, A.: Cuprite, paramelaconite and tenorite films deposited by reactive magnetron sputtering. Appl. Surf. Sci. **210**, 359–367 (2003)

15. Balamurugan, B., Mehta, B.R.: Optical and structural properties of nanocrystalline copper oxide thin films prepared by activated reactive evaporation. Thin Solid Films **396**, 90–96 (2001)

16. Ghosh, S., Avasthi, D.K., Shah, P., Ganesan, V., Gupta, A., Sarangi, D., Bhattacharya, R., Assmann, W.: Deposition of thin films of different oxides of copper by RF reactive sputtering and their characterization. Vacuum **57**, 377–385 (2000)

17. Yoon, K.H., Choi, W.J., Kang, D.H.: Photoelectrochemical properties of copper oxide thin films coated on an *n*-Si substrate. Thin Solid Films **372**, 250–256 (2000)

18. Muthe, K.P., Vyas, J.C., Narang, S.N., Aswal, D.K., Gupta, S.K., Bhattacharya, D., Pinto, R., Kothiyal, G.P., Sabharwal, S.C.: A study of the CuO phase formation during thin film deposition by molecular beam epitaxy. Thin Solid Films **324**, 37–43 (1998)

19. Santra, K., Sarker, C.K., Mukherjee, M.K., Ghosh, B.: Copper oxide thin films grown by plasma evaporation method. Thin Solid Films **213**, 226–229 (1992)

20. Maruyama, T.: Copper oxide thin films prepared by chemical vapor deposition from copper dipivaloylmethanate. Sol. Energy Mater. Sol. Cells **56**, 85–92 (1998)

21. Warren, B.E.: X-ray Diffraction. Addison Wesley Publishing Co., London (1969)

22. Savaloni, H., Player, M.A., Gu, E., Marr, G.: Influence of substrate temperature, deposition rate, surface texture and material on the structure of uhv deposited erbium films. Vacuum **43**, 965–980 (1992)

23. vander Kolk, G.J., Verkerk, M.J.: Microstructural studies of the growth of aluminum films with water contamination. J. Appl. Phys. **59**, 4062–4067 (1986)

24. Khojier, K., Savaloni, H., Kangarloo, H., Ghorannneviss, M., Yari, M.: Influence of annealing temperature on the nanostructure and corrosivity of Ti/stainless steel substrates. Appl. Surf. Sci. **254**, 2528–2533 (2008)

25. Aspnes, D.E., Kinsbron, E., Bacon, D.D.: Optical properties of Au: sample effects. Phys Rev. B **21**, 3290–3299 (1980)